



Photocatalytic TiO₂/rGO/CuO Composite for Wastewater Treatment of Cr(VI) Under Visible Light

Ning Wang · Feiyan Zhang · Qiufeng Mei · Ronglan Wu · Wei Wang

Received: 4 February 2020 / Accepted: 15 April 2020
© The Author(s) 2020

Abstract The harm of chromium pollution to the environment has caused a widespread concern; hexavalent chromium is a toxic, cancerogenic, and genetically mutagenic contaminant to the human body; by contrast, trivalent chromium is almost non-toxic to the human body; therefore, it is a feasible method to reduce hexavalent chromium to trivalent chromium. Photocatalysis is a new environmentally friendly and harmless technology, which can transform pollutants into non-toxic or less toxic products. In this study, we synthesized TiO₂/rGO/CuO ternary nanocomposites to treat hexavalent chromium pollution under visible light. Under optimal conditions, the photoreduction efficiency of 100 ppm hexavalent chromium solution could reach 100% in 80 min. The photoreduction rate of hexavalent chromium is 29.4 times than that of pure TiO₂. The photocatalytic property of CuO in TG2C8 nanocomposites is attributed to accelerate the separation of electrons and holes and the efficient electron transfer through the rGO framework. We believe that TiO₂/rGO/CuO composites have great potential in wastewater treatment.

Keywords Wastewater treatment · TiO₂ nanorods · CuO nanoparticles · Photocatalysis · Visible light irradiation

1 Introduction

The rapid growth of the battery industry, ceramics, mining, and global plastic production causes pollution of all kinds of heavy metals (Cr, Sb, Au, Ag, Hg, Pb, etc.) which threatens the environment and human health (Zhan et al. 2018; Wang et al., 2018a; Li et al. 2018). Chromium pollution, due to mining, electroplating, pigment production, wood preservation, tanning, and metallurgy, has become a key issue in aquatic ecosystems (Jiang et al. 2019; Guan, et al. 2019; Rahmat et al. 2020). Chromium exists mainly in water in two valence states: hexavalent chromium (Cr(VI)) and trivalent chromium (Cr(III)). By contrast, Cr(VI) is a toxic, cancerogenic, and mutagenic contaminant to creatures (Lyu et al. 2019; Yuan et al. 2019a; Wang et al. 2019). The US Environmental Protection Agency stipulates that the maximum concentration of Cr(VI) in surface water is 0.1 ppm and drinking water is 0.05 ppm (Lyu et al. 2019; Qiu et al. 2015). Compared with Cr(VI), Cr(III) is almost non-toxic and is a vital micronutrient for the human body. Cr(III) is easily chelated by natural clay or converted to Cr(OH)₃ and precipitated from water ($K_{sp}(\text{Cr}(\text{OH})_3) = 6.3 \times 10^{-31}$) (Barrera-Diaz et al. 2012; Zhang et al. 2014; Zhang et al. 2018; Wang et al. 2018b). Therefore, it is a

N. Wang · F. Zhang · Q. Mei · R. Wu (✉)
Key Laboratory of Oil & Gas Fine Chemicals, College of
Chemistry and Chemical Engineering of Xinjiang University,
Urumqi 830046, China
e-mail: wuronglan@163.com

W. Wang (✉)
Department of Chemistry & Center for Pharmacy, University of
Bergen, 5020 Bergen, Norway
e-mail: wei.wang@uib.no

feasible method to reduce Cr(VI) to Cr(III). Liang et al. synthesized Ag/ZnO@CF with a 3D hierarchical porous structure, which exhibited significant photocatalysis activity because of the enhanced mass transfer and cocatalyst-facilitated charge separation, and the Ag/ZnO@CF could remove 54.54% of Cr(VI) (20 mg mL⁻¹) from wastewater after 3 h (Liang et al. 2020). Wang et al. synthesized CoS₂/g-C₃N₄-rGO nanocomposites by a one-pot solvothermal method, and 99.8% of Cr(VI) (20 mg mL⁻¹) can be reduced within 120 min (Wang et al. 2020).

Photocatalytic technology is a new environmentally friendly technology to convert pollutants in wastewater into harmless products (Froschl et al. 2012; Wang et al. 2009; Setvin et al. 2013). Semiconductor materials recently emerge as efficient heterogeneous photocatalysts. As a chemically stable, non-toxic, and non-polluting semiconductor material (Chen et al. 2017; Lv et al. 2019; Fan et al. 2019; Kumar et al. 2019), TiO₂ exhibits excellent performance in photocatalysis (Barkhade and Banerjee 2019; Zielińska-Jurek et al. 2017; Yang et al. 2019; Noreen et al. 2019). However, due to its high electron-hole pair recombination rate and the low utilization of visible light, its application in real life is greatly limited (Liu et al. 2020; Kar et al. 2019; Méndez-Medrano et al. 2016). The problem can be solved by extending the range of optical response, for example, coupling with narrow bandgap semiconductors (Mei et al. 2019; Tahir et al. 2019). CuO is a low-bandgap p-type semiconductor material that is cheap and non-toxic. It also has good optical, electrical, and catalytic properties with a narrow energy gap of 1.2–1.7 eV (de Brito et al. 2018; Méndez-Medrano et al., 2016; Mosleh et al. 2018; Chauhan et al. 2019). Graphene is the most emerging material in the current decade. In recent years, graphene has been applied to photocatalytic materials, due to its large surface area, high electron mobility, strong adsorption capacity, and easy chemical modification (Kamat, 2011; Yuan et al. 2019b; Guo et al. 2019).

In this study, we used the advantages of CuO, combining with GO, and synthesized TiO₂/rGO/CuO nanocomposites by a hydrothermal method. CuO can make electron-hole pairs separate faster, and the rGO framework can make electron transfer

faster. We evaluated the photocatalytic property of the catalyst by testing the reduction performance of Cr(VI), and the results show that the TiO₂/rGO/CuO nanocomposites showed excellent property under visible light.

2 Experimental Methods

2.1 Materials

Graphite powders (325 mesh) and titanium dioxide (TiO₂, 99.0%) were purchased from Aladdin Corp (Shanghai, China). Sulfuric acid (H₂SO₄) and phosphoric acid (H₃PO₄) were purchased from Fengchuan Chemical Reagent Co., Ltd. (Tianjin, China). KOH, NaOH, HCl (37%), ethanol, CuSO₄·5H₂O, NH₃·H₂O, K₂Cr₂O₇, NaNO₃, acetone, H₂O₂ (30%), and KMnO₄ were purchased from Zhiyuan Chemical Co., Ltd. (Tianjin, China). They were used as received. Deionized water was used in all experiments.

2.2 Preparation of GO and TiO₂ NRs

TiO₂ nanorods (NRs) were synthesized by a hydrothermal method. TiO₂ (3 g) was dispersed in a KOH solution (10 mol L⁻¹) and stirred. Then, the mixture was transferred to a 100 mL autoclave, which was heated up to 180 °C for 24 h, then washed the product with water and ethanol to remove impurities, then dried the composite, and annealed in a muffle furnace at 500 °C for 4 h, and white TiO₂ powder was obtained. Graphene oxide (GO) was prepared by the same method as that in the reference (Cao et al. 2018). The calculated concentration of GO is 5 mg mL⁻¹.

2.3 Preparation of TiO₂/rGO/CuO

TiO₂/rGO/CuO (TGC) nanocomposites were prepared by a hydrothermal method. GO aqueous solution (0.2 mL, 5.0 mg mL⁻¹) was well dispersed into deionized water (10 mL) by ultrasonic treatment for 30 min. CuSO₄·5H₂O (0.08 g) and TiO₂ NRs (0.2 g) were added to the dispersion, and then continued stirring for 240 min, forming a stable gray suspension. Subsequently, NH₃·H₂O (0.3 mL) and NaOH (4.0 mL, 0.1 g mL⁻¹) solutions were added to the above suspension. Afterward, the above mixture was placed in a 25-mL autoclave, which was heated up to 140 °C for 4 h, and then

washed the composite with deionized water and ethanol to pH = 7, then dried the composites and annealed up to 400 °C for 2 h in an Ar atmosphere.

In comparison, a series of products with additive amount of $\text{CuSO}_4 \cdot 5\text{H}_2\text{O}$ and GO were prepared in the same way. The composite is denoted as TG_xC_y , where x and y represent the amount of GO aqueous solution in volume and $\text{CuSO}_4 \cdot 5\text{H}_2\text{O}$ in weight, respectively and compared their photocatalytic property. The reagent composition of the samples is shown in Table 1.

2.4 Characterization of $\text{TiO}_2/\text{rGO}/\text{CuO}$ Nanocomposites

The crystal structure was recorded by an X-ray diffractometer (XRD, Rigaku Ultima IV, Japan) with $\text{Cu K}\alpha$ source radiation ($\lambda = 0.1542$ nm). The bonding information of the composites was confirmed by X-ray photoelectron spectroscopy (XPS, ESCALAB 250Xi, American Thermo Fisher Scientific) equipped with $\text{Al K}\alpha$ radiation (1486.6 eV). The chemical compositions of the composites were examined by Fourier transform infrared (FTIR, Prestige-21, Shimadzu, Japan) spectroscopy. Measurements of Raman spectra were performed on an XperRam Compac Raman spectrometer with excitation laser beam wavelength of 532 nm. The morphology of composites was captured by scanning electron microscopy (SEM, S-4800 Hitachi, Japan) and high-resolution transmission electron microscopy (HR-TEM, FEITecni G2 F20, America) with an HAADF detector. The absorbance was tested by a UV-Vis spectrometer (UV-2550, Shimadzu). The UV-Vis diffuse reflectance spectra (UV-vis DRS) of the nanocomposites in the range of 250–800 nm were measured by using a U-3010 spectrophotometer with BaSO_4 as a reference.

Table 1 Reagent composition of the samples

	GO (mL)	$\text{CuSO}_4 \cdot 5\text{H}_2\text{O}$ (g)	TiO_2 (g)
TG1C8	0.1	0.08	0.2
TG2C8	0.2	0.08	0.2
TG3C8	0.3	0.08	0.2
TG4C8	0.4	0.08	0.2
TG2C0	0.2	0	0.2
TG2C4	0.2	0.04	0.2
TG2C16	0.2	0.16	0.2

2.5 Photocatalytic Reduction of Cr(VI)

The method of reducing Cr(VI) is the same as that of Mei et al. (2019).

3 Results and Discussion

3.1 XRD

XRD results (Fig. 1) for the TGC samples confirm the presence of CuO crystallites (JCPDS 41–0254) (Zhang et al. 2008) and TiO_2 in anatase phase (JCPDS 21–1272) (Wang et al. 2011). Two peaks at $2\theta = 35.8^\circ$ and 38.4° in the XRD pattern correspond to CuO, which are the (002) and (101) planes, respectively. The strength of these characteristic peaks was significantly enhanced with the increase of added $\text{CuSO}_4 \cdot 5\text{H}_2\text{O}$. However, the characteristic peak of GO was not found on XRD, because the amount of GO is too small and the insertion

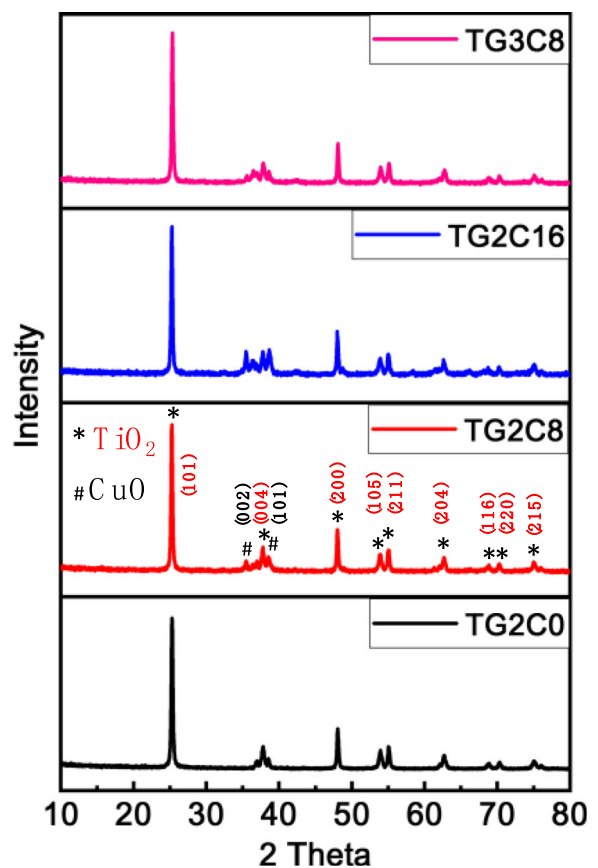


Fig. 1 XRD patterns of TG3C8, TG2C16, TG2C8, and TG2C0

of TiO₂ and CuO destroyed the conventional accumulation of rGO.

3.2 FTIR and Raman

The FTIR spectrum (Fig. 2a) of TG2C8 exhibits characteristic vibrations at 3430 cm⁻¹ (OH stretch) and 1580 cm⁻¹ (OH in-plane bend) for TiO₂ (Chen et al. 2010), the skeleton vibration of GO is at 2320 cm⁻¹; the stretching vibration of CuO bond is at 470 cm⁻¹ (Gusain et al. 2016). The Raman spectrum of TG2C8 (Fig. 2b) shows a characteristic peak of CuO at 276 cm⁻¹, at the same time. TiO₂ peaks can be found at 360, 445, and 660 cm⁻¹. In the Raman spectra, the characteristic peaks at 1351 cm⁻¹ and 1589 cm⁻¹ are corresponding to the D and G peaks of graphene, respectively. These two peaks feature sp³ defects and amorphous structure of carbon atoms of graphene (D peak) and sp²-bonded carbon atoms in the plane (G peak) (Perera et al. 2012; Zhang et al. 2010).

3.3 XPS

The surface bonding state of the composite material is evaluated by XPS analysis (Nguyen et al. 2019). The survey spectrum (Fig. 3a) of TG2C8 shows the photoelectron peaks of titanium, oxygen, carbon, and copper. In the Ti 2p spectra of TG2C8 (Fig. 3b), the Ti 2p_{1/2}(464.1 eV) and Ti 2p_{3/2}(458.5 eV) (Δ BE = 5.6 eV) belong to Ti(IV) (Mei et al. 2019). In the Cu 2p spectra of TG2C8 (Fig. 3c), the Cu 2p_{1/2} (954.2 eV) and Cu 2p_{3/2}(934.2 eV) (Δ BE = 20.0 eV) belong to Cu(II) (Shi et al. 2019). The C 1s spectrum (Fig. 3d) of TG2C8 displays two components at 284.8 eV and

288.3 eV. C–H and C–C carbons of rGO skeleton at 284.8 eV, and the peak at about 288.3 eV belong to C=O of rGO (Tung et al. 2012).

3.4 SEM and TEM

In the SEM (Fig. 4a) and HRTEM (Fig. 4b) images of TG2C8, we observed the TiO₂ nanorods in complex with CuO nanoparticles. The observation on a smaller scale as in Fig. 4c and d shows the interplanar fringes of TiO₂ and CuO. We can clearly identify the lattice of both anatase TiO₂ and CuO. In Fig. 4c, the obvious lattice spacings of about 0.35 nm prove the existence of {101} face of anatase TiO₂ (Shi et al. 2019). In Fig. 4d, a spacing of about 0.23 nm was identified, belonging to the {111} face of CuO (Kumar and Chowdhury 2017), and we also observed the lattice spacings of 0.35 and 0.47 nm with an included angle of 70°, showing the {101} face of TiO₂ (Kumar and Chowdhury 2017). Since the amount of rGO is relatively small, the trace of rGO was not obvious under the electron microscope; however, the Raman spectrum and XPS provided strong proof on the presence of rGO.

3.5 UV-Vis DRS

UV-DRS analysis can predict the bandgap of the composite by measuring the light absorbance of the catalyst under visible light (Nguyen et al. 2019). The UV-Vis absorption spectrum is shown in Fig. 5a. TiO₂ has strong absorption below 400 nm, which is due to the absorption of ultraviolet light by TiO₂ (de Brito et al. 2018). In contrast, CuO and TGC show extensive adsorption in the visible light region.

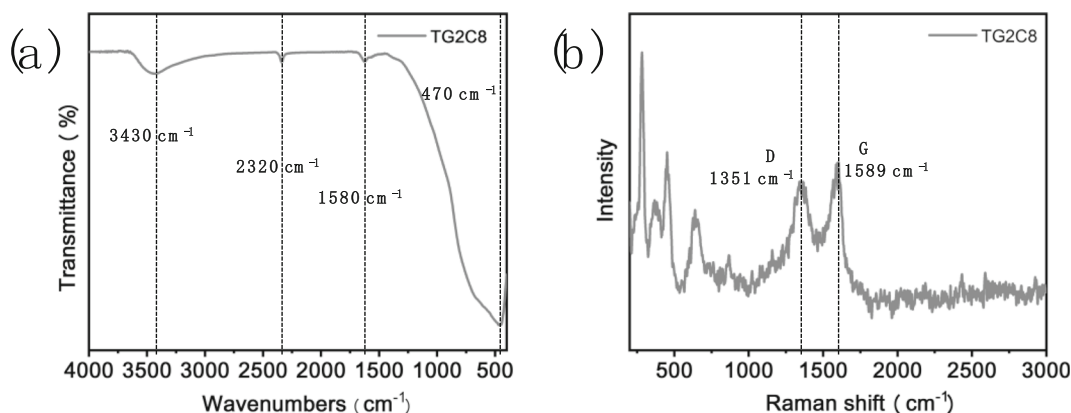


Fig. 2 a FTIR spectra and b Raman spectra of TG2C8

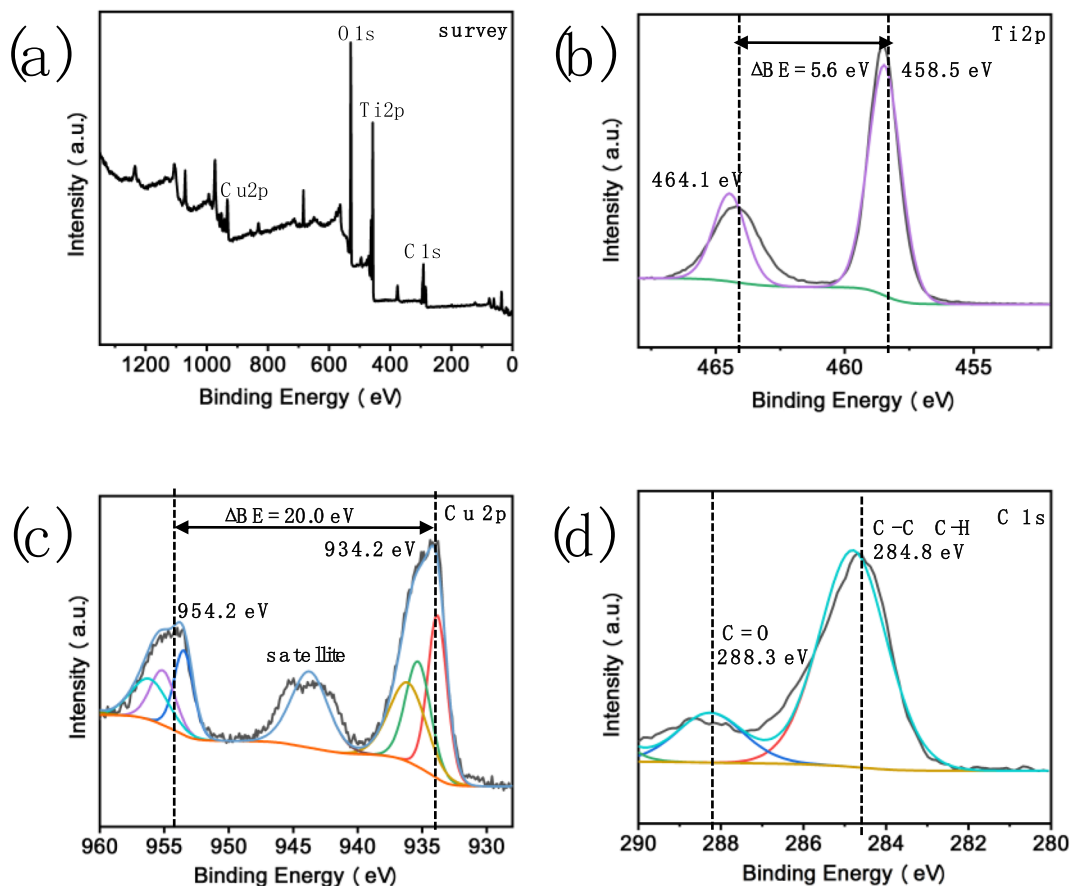


Fig. 3 a The survey spectra of TG2C8, b Ti 2p, c Cu 2p, and d C 1s

The bandgap energy of the CuO, TiO₂, and TGC nanocomposites is shown in Fig. 5b. The bandgap energy is calculated by the Tauc equation (Viezbicke et al. 2015; Mansingh et al. 2017):

$$\alpha h\nu = A(h\nu - E_g)^n$$

where E_g is the energy of bandgap, A is a proportionality constant, $h\nu$ is the approximate bandgap, α is the absorption coefficient, and n equals to 0.5 and 2, corresponding to the direct and indirect transitions, respectively. Both TiO₂ (Zhang et al. 2016) and CuO (Lim et al. 2012) have an indirect bandgap. The calculated bandgap of CuO is about 1.70 eV, the calculated bandgap for TiO₂ (3.2 eV) corresponds to anatase TiO₂, and the calculated bandgap for TGC is 2.45 eV. From the above results, TGC nanocomposites broaden the absorption range of TiO₂.

3.6 Photocatalytic Reduction of Cr(VI)

Cr(VI), a model contaminant, was used for evaluating the photocatalytic property of TGC composites. First, in the dark, we stir the suspension for 40 min until the adsorption-desorption equilibrium is reached. The results in Fig. 6a shows that adsorption-desorption equilibrium can be reached in 20 min. We found that TG2C8 has the highest photocatalytic effect on photoreduction of Cr(VI) and the photoreduction conversion can reach 100% within 80 min, whereas only 63.23% and 9.17% of the added Cr(VI) were photoreduced by using neat TiO₂ and P25 as the catalysts in Fig. 6b, respectively. In order to eliminate the influence of Cr(VI), the photocatalytic test of Cr(VI) was carried out under the condition without nanocomposites, as shown in Fig. 6b. The absorbance of pure Cr(VI) is almost unchanged under the same visible light irradiation, so the influence of Cr(VI) can be excluded. The degradation rate constant (k) was calculated by using the simplified Langmuir-

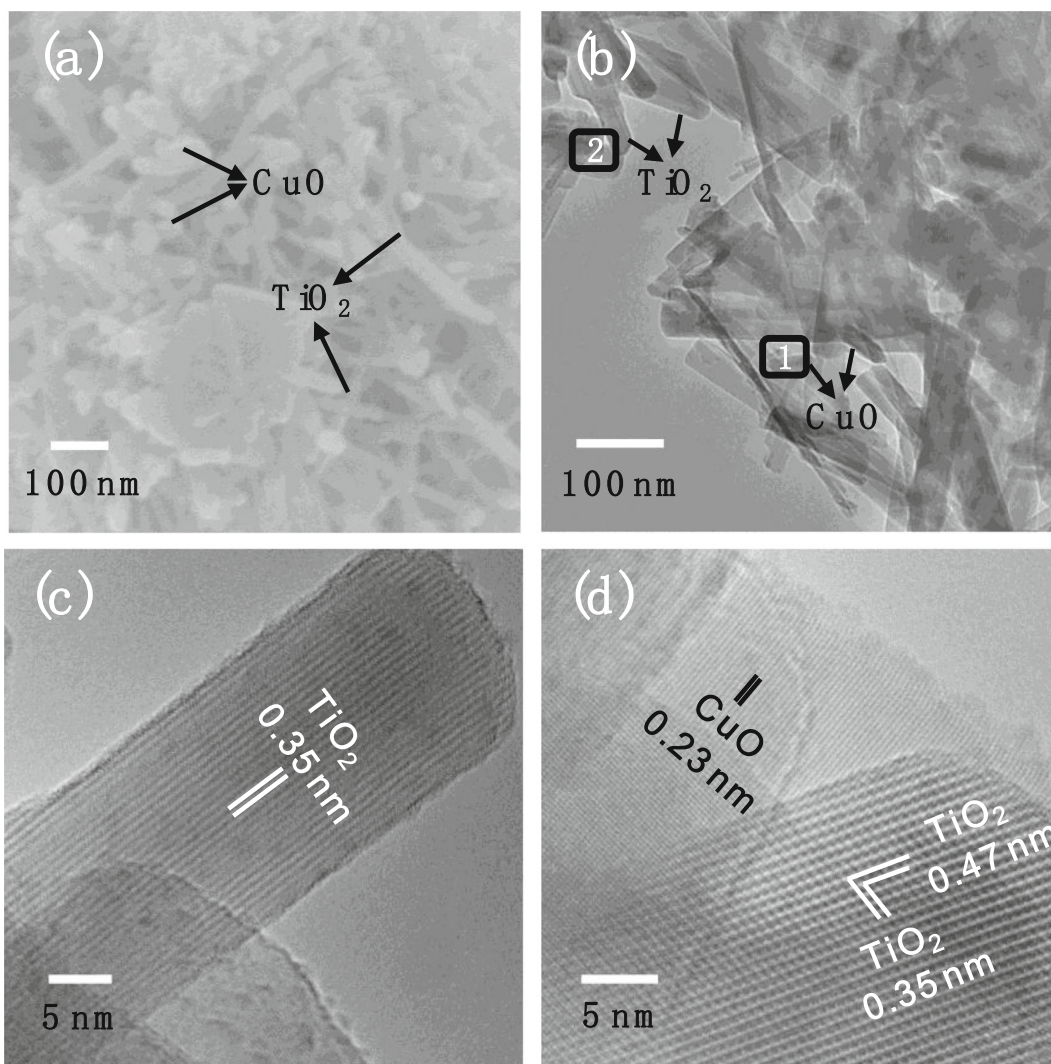


Fig. 4 **a** The SEM image and **b–d** the HRTEM images of TG2C8

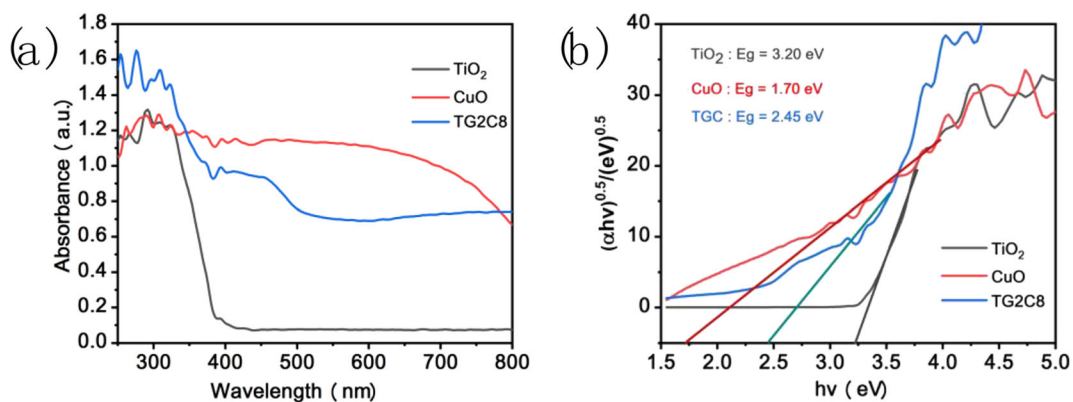


Fig. 5 **a** UV-Vis DRS and **b** $h\nu$ versus $(\alpha h\nu)^{0.5}$ graph of TiO_2 , CuO , and TG2C8

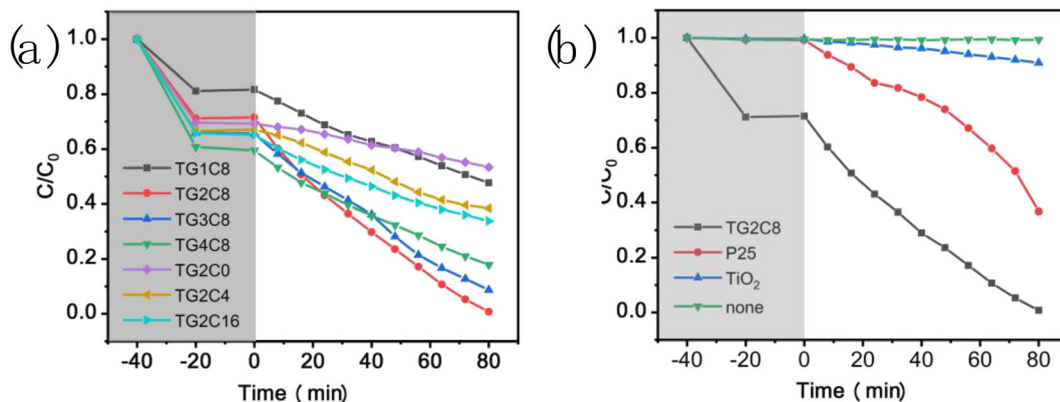


Fig. 6 a The Cr(VI) photoreduction curves of TGC nanocomposites. b The Cr(VI) photoreduction curves of TG2C8, P25, TiO_2 , and blank group

Hinshelwood model (Wang et al. 2006; Jaafarzadeh et al. 2017):

$$\ln \frac{C}{C_0} = -k.t$$

where k is the rate constant (min^{-1}), C_0 is the initial concentration of the Cr(VI), and t is the photodegradation time (min). The calculated rate constant of TG2C8 is 0.0617 min^{-1} , and the calculated rate constants of P25 and TiO_2 were 0.0125 and 0.0021 min^{-1} , respectively. It can be concluded that nanocomposites show excellent photocatalytic property under visible light.

3.7 Plausible Mechanism

We propose a feasible mechanism for the photoreduction of Cr(VI) under visible light, as shown in Fig. 7.

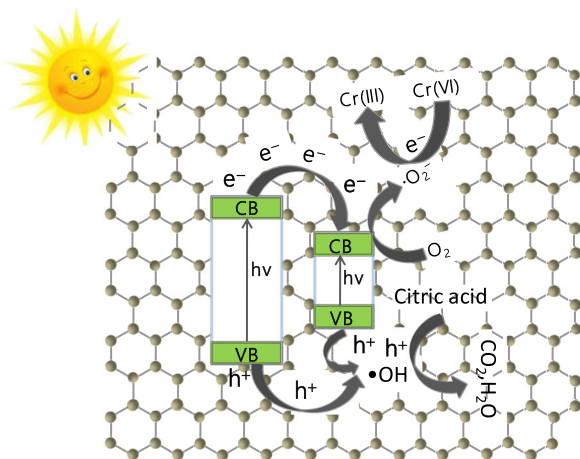


Fig. 7 Plausible mechanism for photoreduction Cr(VI)

Under visible light irradiation, electrons(e^-) are excited to jump to the valence band (VB), leaving holes (h^+) in the conduction band (CB), which results in the formation of electron-hole pairs in TiO_2 . While rGO is used as an electron transfer medium and electron carrier, and the Fermi level of TiO_2 is higher than that of CuO, the photo-excited of TiO_2 will move to the CB of CuO through rGO layer, and the electron-hole pair recombination is inhibited. While e^- converts O_2 to superoxide radicals ($\cdot O_2^-$), Cr(VI) can be reduced by e^- and $\cdot O_2^-$ and e^- . At the same time, the presence of h^+ in the VB of TiO_2 and CuO reacts with H_2O in the reaction medium to form hydroxyl radicals ($\cdot OH$), and citric acid acts as a hole sacrificial agent, which consumes some holes and $\cdot OH$, thereby further accelerating the separation of e^- - h^+ pairs to improve photocatalytic property.

4 Conclusion

CuO nanoparticles and TiO_2 nanorods were grafted onto the rGO framework and then used for photoreduction of Cr(VI), and the introduction of CuO and rGO heightened the absorption of visible light. Under visible light irradiation, TG2C8 can completely reduce the Cr(VI) (100 ppm) solution in 80 min, and the photoreduction conversion rates of Cr(VI) on TG2C8 are 4.9 and 29.4 times those of P25 and pure TiO_2 , respectively. CuO not only accelerates the separation of e^- and h^+ but also reduces the bandgap of TiO_2 . In summary, the improvement in photocatalytic property of TG2C8 composites is attributed to the acceleration of e^- - h^+ pair separation by CuO and the acceleration of effective e^- transfer by rGO.

Funding Information Open Access funding provided by University of Bergen. We thank the financial support of the National Natural Science Foundation of Xinjiang Uyghur Autonomous Region (No. 2016D01C037), the National Natural Science Foundation of China (No. 21868036), the Project of Xinjiang Education Office (No. XJEDU20171004), the Thousand Talent Program, the test platform in the Ministry Key Laboratory of Oil & Gas Fine Chemicals, and the Physical and Chemical Testing Centre of Xinjiang University.

Compliance with Ethical Standards

Conflict of Interest The authors declare that they have no conflict of interest.

Open Access This article is licensed under a Creative Commons Attribution 4.0 International License, which permits use, sharing, adaptation, distribution and reproduction in any medium or format, as long as you give appropriate credit to the original author(s) and the source, provide a link to the Creative Commons licence, and indicate if changes were made. The images or other third party material in this article are included in the article's Creative Commons licence, unless indicated otherwise in a credit line to the material. If material is not included in the article's Creative Commons licence and your intended use is not permitted by statutory regulation or exceeds the permitted use, you will need to obtain permission directly from the copyright holder. To view a copy of this licence, visit <http://creativecommons.org/licenses/by/4.0/>.

References

- Barkhade, T., & Banerjee, I. (2019). Optical properties of Fe doped TiO₂ nanocomposites synthesized by sol-gel technique. *Materials Today: Proceedings*, 18, 1204–1209.
- Barrera-Diaz, C. E., Lugo-Lugo, V., & Bilyeu, B. (2012). A review of chemical, electrochemical and biological methods for aqueous Cr(VI) reduction. *Journal of Hazardous Materials*, 223–224, 1–12.
- Cao, J., Wang, Z., Yang, X., Tu, J., Wu, R., & Wang, W. (2018). Green synthesis of amphipathic graphene aerogel constructed by using the framework of polymer-surfactant complex for water remediation. *Applied Surface Science*, 444, 399–406.
- Chauhan, M., Sharma, B., Kumar, R., Chaudhary, G. R., Hassan, A. A., & Kumar, S. (2019). Green synthesis of CuO nanomaterials and their proficient use for organic waste removal and antimicrobial application. *Environmental Research*, 168, 85–95.
- Chen, C., Cai, W., Long, M., Zhou, B., Wu, Y., Wu, D., & Feng, Y. (2010). Synthesis of visible-light responsive graphene oxide/TiO₂ composites with p/n heterojunction. *ACS Nano*, 4(11), 6425–6432.
- Chen, P., Wang, F., Chen, Z.-F., Zhang, Q., Su, Y., Shen, L., Yao, K., Liu, Y., Cai, Z., Lv, W., & Liu, G. (2017). Study on the photocatalytic mechanism and detoxicity of gemfibrozil by a sunlight-driven TiO₂/carbon dots photocatalyst: the significant roles of reactive oxygen species. *Applied Catalysis B: Environmental*, 204, 250–259.
- de Brito, J. F., Tavella, F., Genovese, C., Ampelli, C., Zanoni, M. V. B., Centi, G., & Perathoner, S. (2018). Role of CuO in the modification of the photocatalytic water splitting behavior of TiO₂ nanotube thin films. *Applied Catalysis B: Environmental*, 224, 136–145.
- Fan, W., Zhou, Z., Wang, W., Huo, M., Zhang, L., Zhu, S., Yang, W., & Wang, X. (2019). Environmentally friendly approach for advanced treatment of municipal secondary effluent by integration of micro-nano bubbles and photocatalysis. *Journal of Cleaner Production*, 237, 117828.
- Froschl, T., Hormann, U., Kubiak, P., Kucerova, G., Pfanzelt, M., Weiss, C. K., Behm, R. J., Husing, N., Kaiser, U., Landfester, K., & Wohlfahrt-Mehrens, M. (2012). High surface area crystalline titanium dioxide: potential and limits in electrochemical energy storage and catalysis. *Chemical Society Reviews*, 41(15), 5313–5360.
- Guan, X., Yang, H., Sun, Y., & Qiao, J. (2019). Enhanced immobilization of chromium(VI) in soil using sulfidated zero-valent iron. *Chemosphere*, 228, 370–376.
- Guo, H., Jiang, N., Wang, H., Shang, K., Lu, N., Li, J., & Wu, Y. (2019). Enhanced catalytic performance of graphene-TiO₂ nanocomposites for synergetic degradation of fluoroquinolone antibiotic in pulsed discharge plasma system. *Applied Catalysis B: Environmental*, 248, 552–566.
- Gusain, R., Kumar, P., Sharma, O. P., Jain, S. L., & Khatri, O. P. (2016). Reduced graphene oxide–CuO nanocomposites for photocatalytic conversion of CO₂ into methanol under visible light irradiation. *Applied Catalysis B: Environmental*, 181, 352–362.
- Jaafarzadeh, N., Ghanbari, F., & Ahmadi, M. (2017). Efficient degradation of 2,4-dichlorophenoxyacetic acid by peroxymonosulfate/magnetic copper ferrite nanoparticles/ozone: a novel combination of advanced oxidation processes. *Chemical Engineering Journal*, 320, 436–447.
- Jiang, B., Gong, Y., Gao, J., Sun, T., Liu, Y., Oturan, N., & Oturan, M. A. (2019). The reduction of Cr(VI) to Cr(III) mediated by environmentally relevant carboxylic acids: state-of-the-art and perspectives. *Journal of Hazardous Materials*, 365, 205–226.
- Kamat, P. V. (2011). Graphene-based nanoassemblies for energy conversion. *The Journal of Physical Chemistry Letters*, 2(3), 242–251.
- Kar, P., Zeng, S., Zhang, Y., Vahidzadeh, E., Manuel, A., Kisslinger, R., Alam, K. M., Thakur, U. K., Mahdi, N., Kumar, P., & Shankar, K. (2019). High rate CO₂ photoreduction using flame annealed TiO₂ nanotubes. *Applied Catalysis B: Environmental*, 243, 522–536.
- Kumar, K., & Chowdhury, A. (2017). Facile synthesis of CuO nanorods obtained without any template and/or surfactant. *Ceramics International*, 43(16), 13943–13947.
- Kumar, A., Khan, M., Fang, L., & Lo, I. M. C. (2019). Visible-light-driven N-TiO₂@SiO₂@Fe₃O₄ magnetic nanophotocatalysts: synthesis, characterization, and photocatalytic degradation of PPCPs. *Journal of Hazardous Materials*, 370, 108–116.
- Li, J., Wang, X., Zhao, G., Chen, C., Chai, Z., Alsaedi, A., Hayat, T., & Wang, X. (2018). Metal-organic framework-based materials: superior adsorbents for the capture of toxic and

- radioactive metal ions. *Chemical Society Reviews*, 47(7), 2322–2356.
- Liang, H., Li, T., Zhang, J., Zhou, D., Hu, C., An, X., Liu, R., & Liu, H. (2020). 3-D hierarchical Ag/ZnO@CF for synergistically removing phenol and Cr(VI): heterogeneous vs. homogeneous photocatalysis. *Journal of Colloid and Interface Science*, 558, 85–94.
- Lim, Y.-F., Choi, J. J., & Hanrath, T. (2012). Facile synthesis of colloidal CuO nanocrystals for light-harvesting applications. *Journal of Nanomaterials*, 2012(7), 1–6.
- Liu, Q., Zhang, J., Xing, F., Cheng, C., Wu, Y., & Huang, C. (2020). Plasmon-enhanced and controllable synthesis of azobenzene and hydrazobenzene using Au/TiO₂ composite. *Applied Surface Science*, 500, 144214.
- Lv, N., Li, Y., Huang, Z., Li, T., Ye, S., Dionysiou, D. D., & Song, X. (2019). Synthesis of GO/TiO₂/Bi₂WO₆ nanocomposites with enhanced visible light photocatalytic degradation of ethylene. *Applied Catalysis B: Environmental*, 246, 303–311.
- Lyu, W., Wu, J., Zhang, W., Liu, Y., Yu, M., Zhao, Y., Feng, J., & Yan, W. (2019). Easy separated 3D hierarchical coral-like magnetic polyaniline adsorbent with enhanced performance in adsorption and reduction of Cr(VI) and immobilization of Cr(III). *Chemical Engineering Journal*, 363, 107–119.
- Mansingh, S., Padhi, D. K., & Parida, K. M. (2017). Enhanced visible light harnessing and oxygen vacancy promoted N, S co-doped CeO₂ nanoparticle: a challenging photocatalyst for Cr(vi) reduction. *Catalysis Science & Technology*, 7(13), 2772–2781.
- Mei, Q., Zhang, F., Wang, N., Yang, Y., Wu, R., & Wang, W. (2019). TiO₂/Fe₂O₃ heterostructures with enhanced photocatalytic reduction of Cr(vi) under visible light irradiation. *RSC Advances*, 9(39), 22764–22771.
- Méndez-Medrano, M. G., Kowalska, E., Lehoux, A., Herissan, A., Ohtani, B., Bahena, D., Briois, V., Colbeau-Justin, C., Rodríguez-López, J. L., & Remita, H. (2016). Surface modification of TiO₂ with Ag nanoparticles and CuO nanoclusters for application in photocatalysis. *The Journal of Physical Chemistry C*, 120(9), 5143–5154.
- Mosleh, S., Rahimi, M. R., Ghaedi, M., Dashtian, K., & Hajati, S. (2018). Sonochemical-assisted synthesis of CuO/Cu₂O/Cu nanoparticles as efficient photocatalyst for simultaneous degradation of pollutant dyes in rotating packed bed reactor: LED illumination and central composite design optimization. *Ultrasonics Sonochemistry*, 40(Pt A), 601–610.
- Nguyen, D. C. T., Cho, K. Y., & Oh, W.-C. (2019). Mesoporous CuO-graphene coating of mesoporous TiO₂ for enhanced visible-light photocatalytic activity of organic dyes. *Separation and Purification Technology*, 211, 646–657.
- Noreen, Z., Khalid, N. R., Abbasi, R., Javed, S., Ahmad, I., & Bokhari, H. (2019). Visible light sensitive Ag/TiO₂/graphene composite as a potential coating material for control of *Campylobacter jejuni*. *Materials Science & Engineering. C, Materials for Biological Applications*, 98, 125–133.
- Perera, S. D., Mariano, R. G., Vu, K., Nour, N., Seitz, O., Chabal, Y., & Balkus, K. J. (2012). Hydrothermal synthesis of graphene-TiO₂ nanotube composites with enhanced photocatalytic activity. *ACS Catalysis*, 2(6), 949–956.
- Qiu, B., Wang, Y., Sun, D., Wang, Q., Zhang, X., Weeks, B. L., O'Connor, R., Huang, X., Wei, S., & Guo, Z. (2015). Cr(vi) removal by magnetic carbon nanocomposites derived from cellulose at different carbonization temperatures. *Journal of Materials Chemistry A*, 3(18), 9817–9825.
- Rahmat, S. T., Tan, W. K., Kawamura, G., Matsuda, A., & Lockman, Z. (2020). Synthesis of rutile TiO₂ nanowires by thermal oxidation of titanium in the presence of KOH and their ability to photoreduce Cr(VI) ions. *Journal of Alloys and Compounds*, 812, 152094.
- Setvin, M., Aschauer, U., Scheiber, P., Li, Y. F., Hou, W., Schmid, M., Selloni, A., & Diebold, U. (2013). Reaction of O₂ with subsurface oxygen vacancies on TiO₂ anatase (101). *Science*, 341(6149), 988–991.
- Shi, Q., Ping, G., Wang, X., Xu, H., Li, J., Cui, J., Abroshan, H., Ding, H., & Li, G. (2019). CuO/TiO₂ heterojunction composites: an efficient photocatalyst for selective oxidation of methanol to methyl formate. *Journal of Materials Chemistry A*, 7(5), 2253–2260.
- Tahir, M. B., Sagir, M., & Shahzad, K. (2019). Removal of acetylsalicylate and methyl-theobromine from aqueous environment using nano-photocatalyst WO₃-TiO₂@g-C₃N₄ composite. *Journal of Hazardous Materials*, 363, 205–213.
- Tung, T. T., Castro, M., Kim, T. Y., Suh, K. S., & Feller, J.-F. (2012). Graphene quantum resistive sensing skin for the detection of alteration biomarkers. *Journal of Materials Chemistry*, 22(40), 21754.
- Viezbicke, B. D., Patel, S., Davis, B. E., & Birnie, D. P. (2015). Evaluation of the Tauc method for optical absorption edge determination: ZnO thin films as a model system. *Physica Status Solidi (B)*, 252(8), 1700–1710.
- Wang, X. H., Li, J. G., Kamiyama, H., Moriyoshi, Y., & Ishigaki, T. (2006). Wavelength-sensitive photocatalytic degradation of methyl orange in aqueous suspension over iron(III)-doped TiO₂ nanopowders under UV and visible light irradiation. *The Journal of Physical Chemistry. B*, 110(13), 6804–6809.
- Wang, N., Zhu, L., Huang, Y., She, Y., Yu, Y., & Tang, H. (2009). Drastically enhanced visible-light photocatalytic degradation of colorless aromatic pollutants over TiO₂ via a charge-transfer-complex path: a correlation between chemical structure and degradation rate of the pollutants. *Journal of Catalysis*, 266(2), 199–206.
- Wang, G., Huang, J., Chen, S., Gao, Y., & Cao, D. (2011). Preparation and supercapacitance of CuO nanosheet arrays grown on nickel foam. *Journal of Power Sources*, 196(13), 5756–5760.
- Wang, Z., Yang, J., Li, Y., Zhuang, Q., & Gu, J. (2018b). In situ carbothermal synthesis of nanoscale zero-valent iron functionalized porous carbon from metal-organic frameworks for efficient detoxification of chromium(VI). *European Journal of Inorganic Chemistry*, 2018(1), 23–30.
- Wang, D., Zhang, G., Dai, Z., Zhou, L., Bian, P., Zheng, K., Wu, Z., & Cai, D. (2018a). Sandwich-like nanosystem for simultaneous removal of Cr(VI) and Cd(II) from water and soil. *ACS Applied Materials & Interfaces*, 10(21), 18316–18326.
- Wang, C. X., Xia, Y. P., Yao, Z. Q., Xu, J., Chang, Z., & Bu, X. H. (2019). Two luminescent coordination polymers as highly selective and sensitive chemosensors for Cr(VI)-anions in aqueous medium. *Dalton Transactions*, 48(2), 387–394.
- Wang, Y., Bao, S., Liu, Y., Yang, W., Yu, Y., Feng, M., & Li, K. (2020). Efficient photocatalytic reduction of Cr(VI) in aqueous solution over CoS₂/gC₃N₄-rGO nanocomposites under visible light. *Applied Surface Science*, 510, 145495.

- Yang, J., Du, J., Li, X., Liu, Y., Jiang, C., Qi, W., Zhang, K., Gong, C., Li, R., Luo, M., & Peng, H. (2019). Highly hydrophilic TiO₂ nanotubes network by alkaline hydrothermal method for photocatalysis degradation of methyl orange. *Nanomaterials (Basel)*, *9*(4), 526.
- Yuan, R., Yue, C., Qiu, J., Liu, F., & Li, A. (2019a). Highly efficient sunlight-driven reduction of Cr(VI) by TiO₂@NH₂-MIL-88B(Fe) heterostructures under neutral conditions. *Applied Catalysis B: Environmental*, *251*, 229–239.
- Yuan, L., Zhang, C., Zhang, X., Lou, M., Ye, F., Jacobson, C. R., Dong, L., Zhou, L., Lou, M., Cheng, Z., Ajayan, P. M., Nordlander, P., & Halas, N. J. (2019b). Photocatalytic hydrogenation of graphene using Pd nanocones. *Nano Letters*, *19*(7), 4413–4419.
- Zhan, Y., He, S., Wan, X., Zhang, J., Liu, B., Wang, J., & Li, Z. (2018). Easy-handling bamboo-like polypyrrole nanofibrous mats with high adsorption capacity for hexavalent chromium removal. *Journal of Colloid and Interface Science*, *529*, 385–395.
- Zhang, X., Wang, G., Liu, X., Wu, J., Li, M., Gu, J., Li, H., & Fang, B. (2008). Different CuO nanostructures: synthesis, characterization, and applications for glucose sensors. *The Journal of Physical Chemistry C*, *112*(43), 16845–16849.
- Zhang, H., Lv, X., Li, Y., Wang, Y., & Li, J. (2010). P25-graphene composite as a high performance photocatalyst. *ACS Nano*, *4*(1), 380–386.
- Zhang, Y. C., Yao, L., Zhang, G., Dionysiou, D. D., Li, J., & Du, X. (2014). One-step hydrothermal synthesis of high-performance visible-light-driven SnS₂/SnO₂ nanoheterojunction photocatalyst for the reduction of aqueous Cr(VI). *Applied Catalysis B: Environmental*, *144*, 730–738.
- Zhang, J., Jin, X., Morales-Guzman, P. I., Yu, X., Liu, H., Zhang, H., Razzari, L., & Claverie, J. P. (2016). Engineering the absorption and field enhancement properties of au-TiO₂ nanohybrids via whispering gallery mode resonances for photocatalytic water splitting. *ACS Nano*, *10*(4), 4496–4503.
- Zhang, H., Li, P., Wang, Z., Cui, W. W., Zhang, Y., Zhang, Y., Zheng, S., & Zhang, Y. (2018). Sustainable disposal of Cr(VI): adsorption–reduction strategy for treating textile wastewaters with amino-functionalized boehmite hazardous solid wastes. *ACS Sustainable Chemistry & Engineering*, *6*(5), 6811–6819.
- Zielińska-Jurek, A., Klein, M., & Hupka, J. (2017). Enhanced visible light photocatalytic activity of Pt/I-TiO₂ in a slurry system and supported on glass packing. *Separation and Purification Technology*, *189*, 246–252.

Publisher's Note Springer Nature remains neutral with regard to jurisdictional claims in published maps and institutional affiliations.